Source-wave angular-momentum effects on electron-diffraction patterns

John J. Barton
IBM Thomas J. Watson Research Center, Yorktown Heights, New York 10598

Louis J. Terminello
Lawrence Livermore National Laboratory, Livermore, California 94550
(Received 20 March 1992)

We use a simple model to predict when electron-emission diffraction patterns from surfaces will have peaks or dips along internuclear axes. A high angular-momentum electron wave emitted from an atom acts like an s wave ($l = 0$) in an extra centrifugal potential. This extra potential changes the electron's effective wave number and phase shift, altering the conditions for constructive interference when this wave scatters from nearby atoms. We demonstrate that the difference in source-wave angular momentum between Cu $M_{2,3}M_{4,5}M_{4,5}$ Auger and Cu $3p$ photoelectrons explains the difference between their emission angular distributions from surfaces: the Auger-electron emission has a predominantly f-like source wave ($l = 3$) and destructive interference in the forward electron-scattering direction ("silhouette") while the photoelectron has lower angular momentum and constructive interference ("peak"). As long as this effect is considered, Auger-electron emission patterns can be used to determine surface structures. The unusual Auger-electron emission patterns observed by Frank *et al.* [Science **247**, 182 (1990)] can be explained as due to high source-wave angular momentum and low electron energy.

Recently,[1] in an attempt to understand the origin of some unusual Auger-electron angular distributions, we demonstrated that isoenergetic (56 eV) Cu $3p$ photoelectrons and Cu $M_{2,3}M_{4,5}M_{4,5}$ Auger electrons from the same Cu(100) single-crystal surface gave quite different experimental angular distribution patterns. Qualitatively, one could characterize the $3p$ photoemission pattern as consisting of a peak along rows of atoms perpendicular to the (100) surface, while the Auger-electron angular distribution pattern along the same emission direction had a dip. What is the origin of this dramatic difference?

At higher electron energies, studies[2] have shown that the features in Auger- and photoelectron emission intensity from surfaces can be described as a "final-state interference" effect. In this model, the angular distribution is dominated by quasiatomic emission, equivalent to that observed for free atoms modified by immersion in a screening medium. The additional detailed features on this smooth background can then be attributed to modifications caused by interference between the atomiclike electron wave function and weaker waves created when this wave scatters from atoms surrounding the emitter. This model has been verified many times, albeit primarily at electron energies above 300 eV.[3,4] While very successful at higher energies, this model would seem to predict similar patterns for atomiclike Auger-electron and atomiclike photoelectron emission from the same crystal at the same electron energy. Within this model we would phrase our question in two parts: (1) Is the quasiatomic model valid for the measured patterns; and (2) if so, what happens to the quasiatomic wave functions at lower energies to make the photoelectron and Auger interference patterns differ?

The first question can be answered simply: we computed the angular distribution for the Cu $3p$ photoelectron and Cu $M_{2,3}M_{4,5}M_{4,5}$ Auger transition using a complete implementation of the quasiatomic model[5] in Fig. 1. Clearly the quasiatomic approximation is valid for these transitions since the theoretical patterns certainly have the same qualitative features as observed experimentally; clearly the quasiatomic model contains the physical ex-

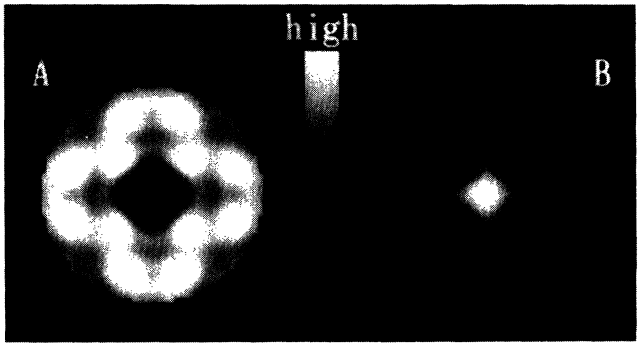

FIG. 1. Calculated electron-emission angular distributions from the Cu(100) surface at $k = 4.1$ Å^{-1}, the internal wave number corresponding to 55 eV external energy, including up to ten sequential multiple scattering events and two orders of spherical wave corrections in the method of Ref. 5. Panel (a), for Cu $M_{2,3}M_{4,5}M_{4,5}$, has an $l = 3$ source wave, each m level equally weighted; panel (b), for Cu $3p$, has a combination of $l = 2$ and $l = 0$ waves weighted and phased as given Ref. 7. The geometry (truncated bulk structure), inelastic mean free path, and thermal damping (Debye temperature: surface 243°, bulk 343°) are identical in both computations.

planation for the differences in the patterns since the theoretical Auger and photoemission patterns are quite different. We can reject the idea of Frank *et al.*[6] that the observations of the dips along interatomic axes in Auger-electron angular distributions provide evidence for anisotropic inelastic scattering. It remains then to answer the second question: why are these patterns different?

For photoemission from core levels (where the quasiatom approximation is valid), dipole selection rules[7] govern the angular-momentum composition of the source wave. For excitation of a core level with angular momentum l_i, the angular integral over the dipole operator, initial core-level orbital, and atomic final state insures that the final state's highest angular momentum will be $l_{f(\max)} = l_i + 1$ and the lowest will be $l_f = l_{f(\max)} - 2$. The azimuthal portion of the same integral gives the magnetic quantum number conservation: $m_f = m_i$. For Cu $3p$ ($l_i = 1$), this gives $l_f = 2, 0$ for each m_i with relative weights and phases given by radial integrals available in standard tables;[7] each initial magnetic level must be considered separately, then averaged to develop the final pattern. At 56 eV, the partial waves $l_f = 2$ and $l_f = 0$ contribute similar amounts to the full wave. However, to simplify our presentation, we ignore the $l_f = 2$ component here and write the photoelectron wave as a simple s wave:

$$\psi_{3p} = h_0(kr) = \frac{e^{ikr}}{ikr}. \tag{1}$$

For Auger emission in the quasiatomic approximation, the source-wave amplitude is given by multipolar selection rules,[8] the angular part of which is similar to the photoemission case. For a transition with initial core hole l_i and final core holes l_1 and l_2, the highest angular momentum will be $l_{f(\max)} = l_i + l_1 + l_2$, the next lowest will be $l_f = l_{f(\max)} - 2$, and so on, in steps of two units to either 0 or 1. The magnetic quantum numbers obey $m_f = m_1 + m_2 - m_i$. For Cu $M_{2,3}M_{4,5}M_{4,5}$, $l_i = 1$, $l_1 = l_2 = 2$, so $l_f = 5, 3, 1$. While we do not know of any standard tables for these Auger matrix elements that relate the population of each of these states to one another, the Cu and Ni $M_{2,3}M_{4,5}M_{4,5}$ transitions have been studied extensively[8,9] and it has been shown that the f wave ($l_f = 3$) dominates. Thus we shall take

$$\psi_{M_{23}M_{45}M_{45},m} = i^3 h_3(kr) Y_{3m}(\hat{r}). \tag{2}$$

Here $i^l h_l(kr)$ is the spherical Hankel function and $Y_{lm}(\hat{r})$ is the spherical harmonic. The only significant difference between this wave function and the photoemission case is the higher angular momentum, and we shall see that this causes the observed differences in the electron-emission patterns.

To illustrate our point it is sufficient to consider only one atom situated between the source and the electron analyzer at a position a with respect to the source atom. The scattered s wave from this atom can be written as[10]

$$\psi_{\rm sc}^{(s)} = \frac{e^{ikR}}{ikR} e^{-ik\mathbf{a}\cdot\mathbf{R}} \frac{e^{ika}}{a} f^{(s)}(k, a, \theta_{aR}). \tag{3}$$

The first term represents the spherical nature of the scattered wave. The next two terms are the geometrical phase terms vital to direct structure methods based upon Fourier analysis of the electron-emission pattern.[11–13] The last term, $f^{(s)}(k, a, \theta aR)$, is a "scattering factor" appropriate for s source waves ($l = 0$) and single scattering,[10] which in the limit of very large internuclear distances tends to the plane-wave scattering factor used in atomic physics.

We also need scattered waves for the higher-angular-momentum f-wave source. Here the expansion coefficients about the scattering center are very much more complicated,[14] and numerous methods have been proposed to simplify them somewhat.[10,15–17] Fortunately a simple physical approximation is adequate for the present purpose. As we show in Fig. 2, an f wave ($l = 3$) differs from an s wave ($l = 0$) in phase, amplitude, and in wavelength, a difference that can be attributed to an additional centrifugal potential for the f wave. If we could shift, scale, and stretch the s wave, then we could use this pseudo-s wave to estimate the scattering of the f wave. The cumulative effect of the centrifugal potential energy, $V_l(r) = l(l+1)/r^2$, can be accurately modeled with an effective wave number,[18]

$$k_{l,r} r = \int_{l+1/2}^{r} \sqrt{k^2 - V_l(r)}\, dr' \approx kr + \frac{(l+1/2)^2}{2kr} - \frac{(l+1/2)\pi}{2}.$$

The result is equivalent to a Jefferys-WKB semiclassical treatment of the difference between h_l and h_0.[19] To use the s-wave equations directly we must make the further approximation of fitting the $k_{l,r}$ at $r = a$ and $r = a/2$ to an r-independent scaled and shifted wave number, giving an effective wave number,

$$k_{l,a} \approx k\left[1 + \frac{(l+1/2)^2}{2(ka)^2}\right], \tag{4}$$

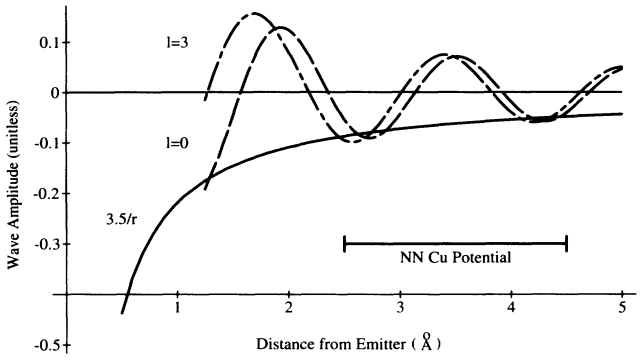

FIG. 2. Sketch of the real part of s-wave ($l = 0$) and f-wave ($l = 3$) source waves [spherical Hankel functions, $i^l h_l(kr)$], for $k = 4$ Å^{-1}. The independent variable r runs from a Cu emitter location at $r = 0$ past the region of the next Cu atom-scattering potential along a (001) direction in a Cu(001) crystal. This region is indicated in the figure centered on $r = 3.5$ Å. Also shown in the figure is the centrifugal potential for the f wave centered on the emitter atom.

in place of k for the source wave in the scattered wave equation,

$$\psi_{sc}^{(f)} \approx \frac{e^{ikR}}{ikR} e^{-ik\mathbf{a}\cdot\mathbf{R}} \frac{e^{ika}}{a} e^{i6/ka} \times f^{(s)}(k_{3,a}, a, \theta_{aR}) Y_3 m(\hat{a}). \quad (5)$$

The effective wave number comes in f and in an exponential phase term where we have approximated $(3 + 1/2)^2/2 \approx 6$.

When the scattered wave is added to the unscattered wave, Eq. (2), and the result is squared and summed over the magnetic quantum number to isolate the interference/geometrical information, the Auger-electron angular distribution (f waves) becomes

$$\chi_{(f)} = \frac{I - I_0}{I_0}$$

$$= P_3(\cos\theta_{aR}) \frac{2\,\mathrm{Re} f^{(s)}(k_{3,a}, a, \theta_{aR}) e^{i6/ka}}{a} \times \cos[k(a - \mathbf{a}\cdot\hat{R})] + \frac{|f^{(s)}(k_{3,a}, a, \theta_{aR})|^2}{a^2}.$$

We have removed $I_0 = 1/(kR)^2$. For s waves we get

$$\chi_{(s)} = \frac{2\,\mathrm{Re} f^{(s)}(k, a, \theta_{aR})}{a} \times \cos[k(a - \mathbf{a}\cdot\hat{\mathbf{R}})] + \frac{|f^{(s)}(k, a, \theta_{aR})|^2}{a^2}.$$

Our simplified model allows us to trace the effect of the source-wave angular momentum on the intensity oscillation in the forward scattering direction ($\theta_{aR} = 0$)

$$\chi_{(f)}(0) = 2\,\mathrm{Re}\left[\frac{f^{(s)}(k_{3,a}, a, 0) e^{i6/ka}}{a}\right] + \frac{|f|^2}{a^2}, \quad (6)$$

$$\chi_{(s)}(0) = 2\,\mathrm{Re}\left[\frac{f^{(s)}(k, a, 0)}{a}\right] + \frac{|f|^2}{a^2}. \quad (7)$$

The f wave has a lower effective wave number, $k_{3,a}$, and an extra energy-dependent phase shift, $e^{i6/ka}$, compared to the s wave.

The difference between the $l = 0$ and $l = 3$ source waves can be expressed as a rotation in the complex plane by $e^{i6/ka}$ and a shift from $f(k, a, 0)$ to $f(k_{3,a}, a, 0)$, as illustrated in Fig. 3. This figure shows a magnified view of the complex plane. Each dot represents a normalized wave amplitude, $\psi/\sqrt{I_0}$ for $\theta = 0$. For an $l = 0$ source wave, this quantity is the complex number $1 + f(k, a, 0)/a$. A portion of the unit circle is also drawn. Since the square of this normalized wave amplitude equals $\chi_{(s)}(0) - 1$, those dots within the unit circle correspond to destructive interference (forward dips) and those dots outside correspond to constructive interference (forward peaks). The bottom set of labeled points near 55 eV ($k = 4$ Å^{-1}) corresponding to the measurements of Ref. 1: the $l = 0$ peak (outside the unit circle) becomes a dip when source-wave phase rotation is included (55 eV on $l = 0$ to 55 eV on $l = 3$), and the dip accentuates with the effective wave number (55 eV on $l = 3$ to 44 eV on $l = 3$). The upper set of points for 462 eV ($k = 11$ Å^{-1}) is too far from the unit circle for the source wave angular momentum to alter the forward peak dramatically (the effective wave-number effect is negligible at this high energy).

The rotation corresponds to the phase difference between the $l = 0$ and $l = 3$ waves at the scattering atom: the extra centrifugal potential delays the $l = 3$ wave, thus leading to destructive interference; the wave-number adjustment accentuates the destructive interference because the real part of $f^{(l=0)}(k)$ decreases with k for $k \approx 4$ Å^{-1} in Cu.

In Fig. 4 we compare the results from electron angular distribution simulations using this model for Cu 56-eV Auger and photoelectrons (using phase shifts and bond lengths appropriate for Cu at 56 eV). The s-wave (photoemission) curve shows the expected forward peak, while the f-wave (Auger) angular distribution has a dip (silhouette). Thus we have demonstrated that the difference between the photoemission and Auger results can be explained with a two-atom model — a simple consequence of their respective source-wave angular momenta.

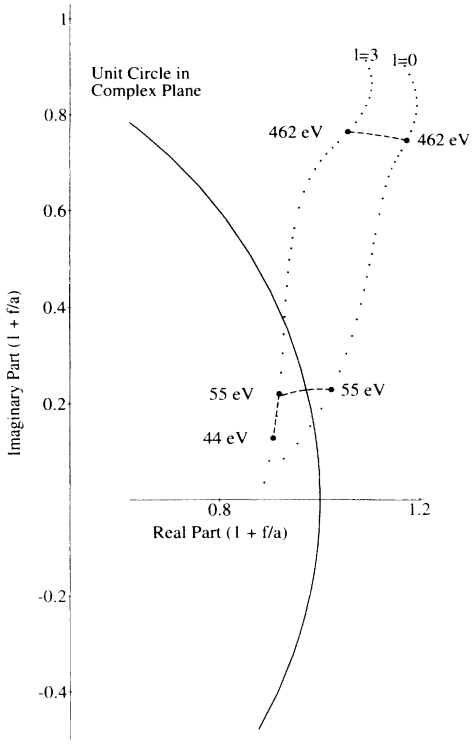

FIG. 3. Illustration of the impact of source wave angular momentum on forward-scattering intensity. Each dot in the track on the right labeled $l = 0$ represents the complex number $1 + f/a$, where $f = f^{(l=0)}(k, a, \theta_{aR})$ and $a = 3.52$, the internuclear distance along a (001) axis in a Cu (001) crystal. The values of k correspond to energies of 34, 39, 44, 49, 55, 61, 67, 74, 81, 88, 95, 103, 111, 119, 128, 137, 161, 187, 214, 244, 275, 309, 344, 381, 461, 549, 644, 747, 857, 975, 1101, 1234, 1375, and 1524 eV, as we move from the bottom to the top of the track. The track on the right, labeled $l = 3$, is the same quantity with f multiplied by $\exp(i6/ka)$.

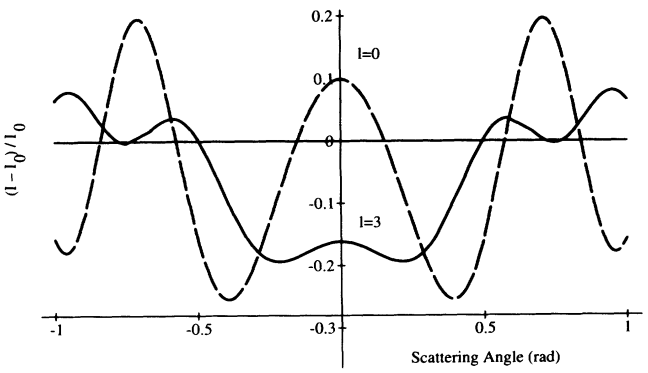

FIG. 4. Photoemission ($l = 0$) and Auger ($l = 3$) electron angular distributions (χ) for Cu at $k = 4$ Å^{-1} using Eq. (6). These curves represent only single elastic scattering in a simplified model and the interference between source and scattered waves. They illustrate that changing source-wave angular momemtum alone converts a forward peak to a dip.

No other considerations[6,20] are needed.

Our model also explains why only forward peaks have been seen in the work done at higher electron energies. As the energy increases, the angular-momentum induced centrifugal potential is less effective and the quantity $|f|^2/a^2$ grows, insuring constructive interference and an intensity-enhanced forward peak.

The low-energy angular distributions for bulk materials need not always appear so clearly as peaks or silhouettes. The additional Legendre polynomial $P_3(\cos\theta_{aR})$ in the f-wave equation reduces the first-order diffraction feature near $\theta_{aR} \approx 0.7$, see Fig. 3. Thus, along the crystal normal, Cu $M_{2,3}M_{4,5}M_{4,5}$ emission will not have first-order diffraction contributions from atoms in the plane directly above the emitter that reinforce the forward peak for Cu $3p$. This makes the difference between the Auger and photopeak angular distributions more dramatic than it might have been. Such complications will not apply to angular distributions from unique atom species in the near surface region, the cases most interesting for the structure determination from angular distribution analysis.

While detailed comparisons to existing experimental data will be required to verify this, this work presents a strong argument that the source-wave angular-momentum effect can explain the varied observations of forward-scattering intensity for Auger electrons that we summarized in Ref. 1. Dips in the forward direction should do the following:

(1) Occur for materials with low wave number, high angular-momentum Auger holes (to get a large centrifugal potential effect).

(2) Occur for Auger transitions that are "quasiatomic" (only atomic effects are needed to generate high-angular-momentum waves).

(3) Not occur for materials with high wave number or low-angular-momentum Auger holes (where centrifugal effects are small).

(4) Not occur for photoemission from low-angular-momentum core levels (unless the wave number is also very low).

(5) Not occur for the angular distribution of emission from atoms on top of surfaces (dips are caused by scattering interference).

(6) Not be predicted by quantum scattering models based upon s-wave continuum waves (must include the centrifugal effect).

(7) Be predicted by quantum scattering models using higher-angular-momentum waves (as indicated here).

We believe that proper consideration of the source-wave angular momentum, which explains the difference between the angular distributions of Cu $M_{2,3}M_{4,5}M_{4,5}$ Auger electrons and the Cu $3p$ photoelectrons, extends the direct analysis of Auger and photoelectron angular distributions from the high-energy "forward-focusing" regime to the lower-energy regime used in the experiments reported by Frank *et al.*[6] The central problem in using Auger-electron angular distributions as a solid-state structural probe remains the determination of the source wave. The Cu $M_{2,3}M_{4,5}M_{4,5}$ Auger transition is one of only a few transitions where the transition matrix elements have been studied.[9] Without some method of estimating the Auger-electron source-wave angular-momentum composition and relative phase shifts, clever empirical work will be needed to fully exploit the potential of these measurements.

We would like to thank J. J. Rehr for help in obtaining the partial-wave phase shifts used in some of these calculations. This work was conducted in part under the auspices of the U.S. Department of Energy by the Lawrence Livermore National Laboratory, under Contract No. W-7405-ENG-48.

[1] L. J. Terminello and J. J. Barton, Science **251**, 1281 (1991).
[2] C. S. Fadley, Prog. Surf. Sci. **16**, 275 (1984).
[3] Z.-L. Han, S. Hardcastle, G. R. Harp, H. Li, X.-D. Wang, J. Zhang, and B. P. Tonner, Surf. Sci. **258**, 313 (1991).
[4] S. A. Chambers, Adv. Phys. **40**, 357 (1991).
[5] J. J. Barton, S. W. Robey, and D. A. Shirley, Phys. Rev. B **34**, 3807 (1986).
[6] D. G. Frank, N. Batina, T. Golden, F. Lu, and A. T. Hubbard, Science **247**, 182 (1990).
[7] S. M. Goldberg, C. S. Fadley, and S. Kono, J. Electron Spectrosc. Relat. Phenom. **21**, 285 (1981).
[8] P. J. Feibelman and E. J. McGuire, Phys. Rev. B **15**, 3575 (1977).
[9] H. L. Davis, in *Proceedings of the 7th International Vacuum Congress and 3rd International Conference on Solid Surfaces, Vienna*, edited by R. Dobrozemsky (Dobrozemsky, Vienna, 1977), p. 2281.
[10] J. J. Barton and D. A. Shirley, Phys. Rev. B **32**, 1906 (1985).
[11] J. J. Barton, Phys. Rev. Lett. **61**, 1356 (1988).
[12] J. J. Barton, J. Electron Spectrosc. **51**, 37 (1990).
[13] J. J. Barton and L. J. Terminello, in *Structure of Surfaces*

III, Milwaukee, edited by S. Y. Tong, M. A. Van Hove, X. Xide, and K. Takayanagi (Springer-Verlag, Berlin, 1991), p. 107.
[14]R. Nozawa, J. Math. Phys. **7**, 1841 (1966).
[15]V. Fritzsche, J. Phys. Condens. Matter **2**, 1413 (1990).
[16]J. J. Barton and D. A. Shirley, Phys. Rev. B **32**, 1892 (1985).
[17]J. J. Rehr and E. A. Albers, Phys. Rev. B **41**, 8139 (1990).
[18]H. S. W. Massey, E. H. S. Burhop, and H. B. Gilbody, *Electronic and Ionic Impact Phenomena* (Oxford University, London, 1969).
[19]R. E. Langer, Phys. Rev. **51**, 669 (1937).
[20]S. A. Chambers, Science **248**, 1129 (1990); W. F. Egelhoff Jr., J. W. Gadzuk, C. J. Powell, and M. A. Van Hove, *ibid.* **248**, 1129 (1990); X. D. Wang, Z. L. Hau, B. P. Tonner, Y. Chen, and S. Y. Tong, *ibid.* **248**, 1129 (1990); D. P. Woodruff, *ibid.* **248**, 1131 (1990).

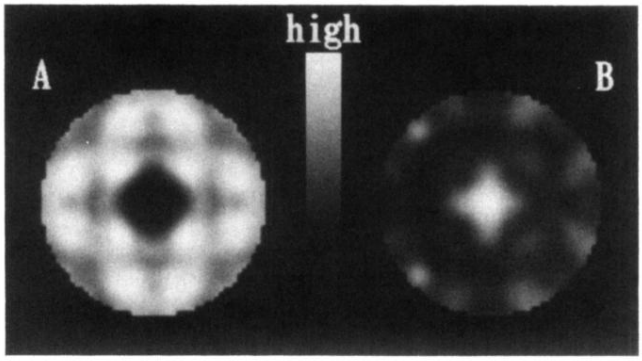

FIG. 1. Calculated electron-emission angular distributions from the Cu(100) surface at $k = 4.1$ Å^{-1}, the internal wave number corresponding to 55 eV external energy, including up to ten sequential multiple scattering events and two orders of spherical wave corrections in the method of Ref. 5. Panel (a), for Cu $M_{2,3}M_{4,5}M_{4,5}$, has an $l = 3$ source wave, each m level equally weighted; panel (b), for Cu $3p$, has a combination of $l = 2$ and $l = 0$ waves weighted and phased as given Ref. 7. The geometry (truncated bulk structure), inelastic mean free path, and thermal damping (Debye temperature: surface 243°, bulk 343°) are identical in both computations.